Mon. Not. R. Astron. Soc. **313**, 21–31 (2000)

Statistical properties of metal abundances of the intracluster medium in the central region of clusters

Y. Fukazawa,[1]★ K. Makishima,[1] T. Tamura,[2] K. Nakazawa,[1] H. Ezawa,[4] Y. Ikebe,[3] K. Kikuchi[4] and T. Ohashi[4]

[1]*Department of Physics, School of Science, University of Tokyo, 7-3-1 Hongo, Bunkyo-ku, Tokyo 113-0033, Japan*
[2]*The Institute of Space and Astronautical Science, 3-1-1 Yoshinodai, Sagamihara, Kanagawa 229-8510, Japan*
[3]*Max-Planck-Institut für Extraterrestrische Physik, Giessenbachstraße, D-85748 Garching, Germany*
[4]*Department of Physics, Faculty of Science, Tokyo Metroplitan University, Hachioji, Tokyo 192-0397, Japan*

Accepted 1999 October 18. Received September 23; in original form 1999 March 10

ABSTRACT

We measured metal abundances of the intracluster medium in the central regions of 34 nearby clusters of galaxies, using *ASCA* data. Clusters that have a sharp X-ray emission centred on a cD galaxy are commonly found to exhibit a central increment in the Fe abundance, which is more pronounced in lower temperature clusters; +(0.1–0.2) solar at $kT > 5$ keV, compared with +(0.2–0.3) solar at $1.5 < kT < 4$ keV. These central excess metals are thought to be ejected from cD galaxies. Several low-temperature cD type clusters also show significant Si abundance increase by +(0.1–0.2) solar at the central region. Compared with the Si-rich abundances observed in the outer regions of rich clusters, the Si to Fe abundance ratio of central excess metals tends to be near the solar ratio, implying that type Ia products from cD galaxies are dominant for the central excess metals. On the other hand, some other clusters do not show the central Fe abundance increase. As these clusters tend to contain two or three central giant galaxies, it is suggested that galaxy interactions have removed the central abundance increase.

Key words: galaxies: abundances – galaxies: clusters: general – galaxies: elliptical and lenticular, cD – X-rays: galaxies.

1 INTRODUCTION

The metal abundances of the intracluster medium (ICM) contain valuable information on the star formation history in galaxies and clusters (Arnaud et al. 1992; Renzini et al. 1993). Based on *ASCA* data, Mushotzky et al. (1996) found that abundance ratios between α elements and iron are about twice as large as the solar ratios, suggesting that a large amount of metals in the ICM was produced by type II supernovae (SNe II). Fukazawa et al. (1998) investigated spatially averaged Si and Fe abundances of nearby 40 clusters, and confirmed the Si-rich abundances among rich clusters. In addition, they found a decrease in the Si to Fe abundance ratio toward low-temperature clusters; from ~2 at the ICM temperature of $kT > 4$ keV to ~1 at $kT \sim 1$ keV. This result indicates significant contribution of type Ia supernovae (SNe Ia) to the metal enrichment of the ICM. Ezawa et al. (1997) found a large-scale Fe abundance gradient in the nearby poor cluster AWM7, which suggests that the metals mostly remain where they were first ejected. Finoguenov & Ponman (1999) found a radial increase of Si to Fe abundance ratios of the ICM, suggesting that the SNe II ejecta have been more widely distributed in the ICM.

Since most metals in the ICM are thought to have been ejected from elliptical galaxies (Arimoto & Yoshii 1987), some evidences of metal ejection were expected around them. *ROSAT*, *BBXRT*, *Ginga* and early *ASCA* observations show, however, that the interstellar media (ISM) in elliptical galaxies have unexpectedly low metal abundances of <0.6 solar (e.g. Awaki et al. 1991, 1994; Loewenstein et al. 1994; Mushotzky et al. 1994). Recent careful analysis of *ASCA* data by Matsushita (1997) and Matsushita et al. (1997) revised these estimates up to ~1 solar in most X-ray-luminous galaxies, and made the ICM abundance consistent with the stellar atmospheric abundances. However, even in such a case, the amount of metals in the ISM of elliptical galaxies is quite low compared with that in the ICM. Thus, most metals in the ISM of elliptical galaxies are thought to have escaped into the vast intergalactic spaces (Tsuru 1992; Matsushita 1997), and few of them are now seen around galaxies themselves.

Most elliptical galaxies in clusters are moving in the ICM, so that the metal-rich products may be stripped off and left behind them. In this respect, central dominant elliptical galaxies (so called 'cD galaxies') are unique objects because they are thought

★ E-mail: fukazawa@amalthea.phys.s.u-tokyo.ac.jp

to sit at the bottom of the cluster potential and are surrounded by the dense ICM. Their environment will therefore give us unique opportunities to search for possible evidence of metal enrichment. *Ginga* and *ASCA* observations have actually led to the discoveries of abundance increases at the centre of several low-temperature clusters (Koyama, Takano & Tawara 1991; Fukazawa et al. 1994; Matsumoto et al. 1996; Xu et al. 1997; Kikuchi et al. 1999). In contrast, some other clusters show spherically uniform abundances at the centre, such as A1060 (Tamura et al. 1996). Consequently, no general view has been constructed as to the metal abundance of the ICM at the cluster centre. Tamura et al. (1996) suggest that clusters with a cD galaxy tend to exhibit the abundance increase at the centre, and those with several dominant galaxies do not. However, this suggestion is yet to be confirmed using a larger sample.

Yamashita (1992) and Fabian et al. (1994a) found, with *EXOSAT* and *Ginga* data respectively, that the emission-weighted Fe abundance of cooling-flow clusters, which exhibit significant X-ray excess emission at the position of a cD galaxy, is higher than that of non-cooling-flow clusters, and this has been confirmed by Allen & Fabian (1998) with *ASCA* data. Allen & Fabian (1998) attributed this tendency to the possible metallicity increase in the centre of 'cooling flow' clusters, but they did not perform spatially resolved spectroscopy.

In this paper, we report systematic measurements of the central metal abundances of the ICM using the imaging spectroscopic capability of *ASCA* (Tanaka, Inoue & Holt 1994), to improve our understanding of the cluster central region and pursue the metal ejection from cD galaxies.

2 OBSERVATIONS AND DATA REDUCTION

As listed in Table 1, we selected 34 nearby bright clusters of galaxies observed by *ASCA* until 1996. These clusters have already been utilized to derive spatially averaged Si and Fe abundances by Fukazawa et al. (1998). Most of these objects are located at redshifts of $z < 0.063$. The original sample is defined in Fukazawa et al. (1998), from which we exclude 6 clusters, for which optical information is not available or the *ASCA* data quality is not enough to resolve the central region.

After Tamura et al. (1996) and Fabian et al. (1994a), we classified our sample clusters into two subsamples in terms of optical and X-ray properties at the centre. One type of object has an extremely bright giant galaxy (cD galaxy) and, hereafter, we call this a cD type cluster; the other type has several giant galaxies at the cluster centre (hereafter a non-cD type cluster). This classification is primarily based on the Rood–Sastry classification (Rood & Sastry 1971; Struble & Rood 1987; Bahcall 1977). Although the Perseus, Centaurus, Virgo, and A262 clusters are optically classified as non-cD type, they exhibit X-ray properties similar to those of cD type clusters; e.g. a sharp X-ray peak centred on one of the central bright galaxies (Jones & Forman 1984) represented by high cooling-flow rates (Fabian, Nulsen & Canizares 1984), and strong spectral cool components (Fabian et al. 1994b; Matsumoto et al. 1996; Fukazawa 1997). These clusters indeed contain quite a central dominant galaxy; for example, M87 in the Virgo cluster. Therefore, we reclassify these four clusters as cD type. In contrast, we reclassify A2634 as non-cD type, because its cD galaxy is now resolved into two crossing giant galaxies (Scott, Robertson & Tarenghi 1977) and its X-ray emission at the centre is very flat, like other non-cD types. The Rood–Sastry classification is not available for A4059, Hydra-A or 2A0335+096. As each of them contains a prominent central dominant galaxy, we include them as cD types. MKW (Morgan et al. 1975) and AWM (Albert et al. 1977) poor clusters of galaxies are grouped into cD types, according to their classification. The NGC 507, Fornax, NGC 5044, and HCG62 groups of galaxies clearly contain central dominant elliptical galaxies that exhibit excess X-ray emission over the group emission, and thus we include them as cD types.

The results of classification are shown in Table 1. Excluding clusters for which no cooling-flow rate is available, all the cD type clusters are reported to have a significant cooling-flow rate (Edge, Stewart & Fabian 1992; White, Jones & Forman 1998). Among non-cD type clusters, A119, A2147 and A1060 are reported to have cooling-flow rates of 38, 88 and $19\,M_{\odot}\,yr^{-1}$, respectively, and the remaining clusters show no significant cooling flow. Therefore, our classification is similar to, but not exactly the same as, that based on the apparent cooling-flow rate.

During *ASCA* observations of these clusters, the GIS (Gas Imaging Spectrometer: Ohashi et al. 1996; Makishima et al. 1996) data were all acquired in the normal PH mode, and most of the SIS (Solid-state Imaging Spectrometer) data were taken in the 4CCD faint/bright mode. The data selections were performed on the condition of a minimum cut-off rigidity of $8\,GeV\,c^{-1}$ and a minimum elevation angle of 5° above the earth rim. For the SIS, we further impose the condition of an elevation angle greater than 25° above the day earth rim, and we use events that have grade 0,

Table 1. The cD and non-cD type classification of our sample clusters. The Rood–Sastry classification is shown in the parentheses.

cD type				
A2319(cD)[a]	A478(cD)[a]	Perseus(L)[a]	A3571(cD)[b]	A85(cD)[a]
A1795(cD)[a]	A3558(cD)[b]	A496(cD)[a]	A2199(cD)[a]	A4059(–)
AWM7[c]	MKW3s[c]	A2063(cD)[a]	Centaurus(I)[b]	Hydra-A(–)
2A0335+096(–)	Virgo(I)[b]	AWM4[c]	A262(C)[a]	MKW4s[c]
MKW4[c]	NGC 507 group[d]	Fornax[d]	NGC 5044 group[d]	HCG62[d]
non-cD type				
Coma(B)[a]	A2256(B)[a]	A119(C)[a]	A2147(F)[a]	A2634(cD)[a]
A1367(F)[a]	A539(F)[a]	A1060(C)[a]	A400(I)[a]	

[a] Struble & Rood (1987).
[b] Bahcall (1977).
[c] Morgan, Kayser & White (1975); Albert, White & Morgan (1977) .
[d] Group of galaxies.

2, 3 or 4. For the spectral analysis, we added all the available data from different sensors, chips, modes and pointings, separately for the GIS and the SIS after an appropriate gain correction. As the SIS data of A119 is severely affected by radiation damage of CCDs, we use only the GIS data and fix the Si abundance to be the same as the Fe abundance.

As *ASCA* has an angular resolution of 1–2 arcmin, the central spectra were integrated within 2 arcmin from the X-ray peak. The statistics of spectra of several clusters are poor within 2 arcmin, and in such cases the integration radius is set to be 3 arcmin (Coma and MKW4s). The background spectra were constructed from several blank-sky data, such as NEP, Draco and QSF-3 fields for a total accumulation time of about 100 ks, integrated over the same region as that of the on-source spectra under the same data selection criteria. As spectra of the Fornax cluster and the NGC 507 group are contaminated by a hard component associated with their cD galaxies, we fit their spectra including a bremsstrahlung component with a temperature of $\sim$10 keV. The flux mixing effect by the point spread function (PSF) of the X-ray Telescope (Takahashi et al. 1995) is negligible for the central spectra because of higher flux at the cluster centre.

For comparison, we utilize the *ASCA* spectra from outer regions of these clusters, which are described by Fukazawa et al. (1998). Throughout this paper, errors represent 90 per cent confidence level, and we assume the Hubble constant to be $50\,h_{50}\,\mathrm{km\,s^{-1}}$ $\mathrm{Mpc^{-1}}$. Solar abundances are taken from the solar photospheric values by Anders & Grevesse (1989), with $(\mathrm{Fe/H})_\odot = 4.68 \times 10^{-5}$ and $(\mathrm{Si/H})_\odot = 3.55 \times 10^{-5}$.

3 RESULTS

3.1 Spectral changes in the central region

Fig. 1, which compares the central spectra with the outer region spectra of two clusters, best exemplifies apparent spectral changes in the radial directions. Here, the central region spectra have been produced as described in Section 2, while the outer region spectra were taken from Fukazawa et al. (1998). The Centaurus cluster exhibits a remarkable spectral change at the centre; the strong Fe L and Fe K lines in its central spectrum, together with strong K lines of other elements, indicate the presence of cool component and the abundance increase, as already reported by Fukazawa et al. (1994), Fabian et al. (1994b) and Ikebe et al. (1999). Several other clusters (Virgo, AWM7, A262 and MKW4) show similar remarkable spectral changes. On the other hand, A2199 shows only a weak, though significant, enhancement of Fe K and Fe L lines at the centre. Many clusters have weaker spectral changes than the Centaurus cluster.

We fit the GIS/SIS central spectra simultaneously with a single-temperature variable abundance Raymond–Smith model (1T R–S model: Raymond & Smith 1977). We set the energy band for the fitting to 0.45–9.0 keV and 0.6–10.0 keV for the SIS and the GIS, respectively. Fukazawa et al. (1998) excluded lower energy bands of $<$0.8 keV and $<$1 keV for the SIS and GIS, respectively, where calibration uncertainties exist. Here we include the lower energy bands, however, because the spectral cool components cannot be well constrained otherwise and calibration uncertainties are often smaller than statistical ones. Free parameters of the fit are the interstellar absorption (N_H), temperature (kT), normalization and abundances of O, Mg, Si, S and Fe. We assume the Ne abundances to be the same as O, Ca and Ar the same as S, and Ni the same as Fe, all in terms of the solar units. The abundances of He, C and N are fixed at the solar values. Here, we focus upon Si and Fe abundances, because other elemental abundances are poorly constrained. The fitting results are shown in Table 2. The fit is generally good, with a reduced χ^2 value of 1.4 or less in most clusters. However, extremely large reduced χ^2 values were obtained in several clusters, meaning that the 1T R–S model is not acceptable.

Compared with the spatially averaged cluster temperature in Fukazawa et al. (1998) obtained by excluding the central region, the central temperature is systematically lower by up to 20 per cent in most clusters, as shown in Fig. 2. Therefore, we confirm

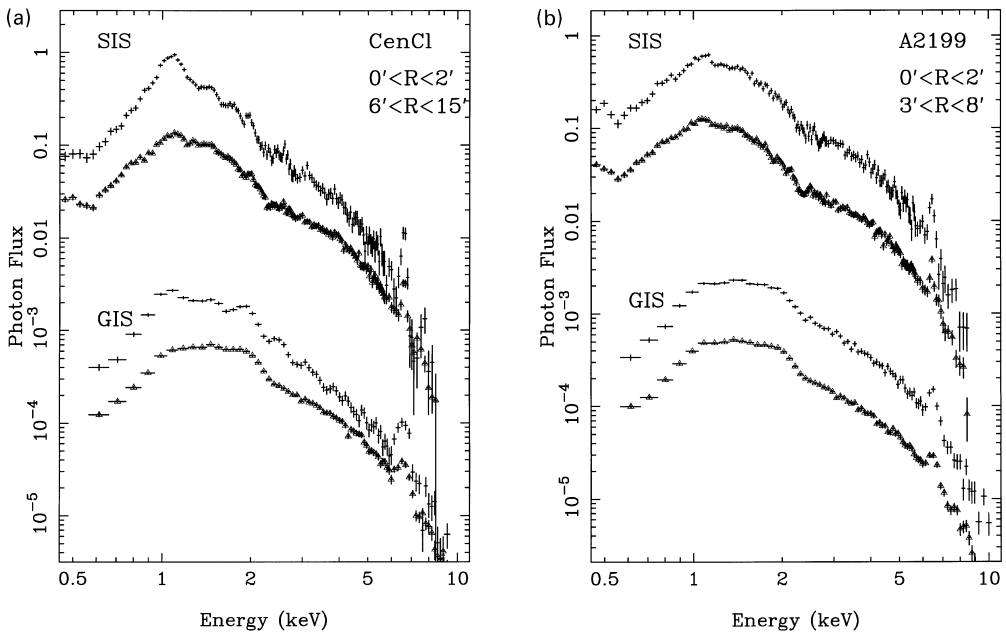

Figure 1. Comparison between the outer region spectra and the central spectra, for the Centaurus cluster (left) and A2199 (right). For each instrument, the upper trace is the central spectrum and the lower is the outer region spectrum.

that the ICM temperature (or its representative value) generally decreases toward the cluster centre, as already reported repeatedly from previous observations (e.g. Fabian et al. 1994a).

The central Fe abundances of most cD type clusters are significantly higher than the outer region values of ∼0.3 solar derived in Fukazawa et al. (1998). However, the abundances may be affected by the cool component; we therefore directly compare the equivalent width (*EW*) of Fe K lines between the central spectra and the outer region spectra to confirm the abundance increase more unambiguously. From Fig. 2, the *EW* of Fe K lines in the central spectra is seen to be about twice as large as that of the outer region spectra for many cD type clusters; ensemble-averaged *EW* enhancements are 1.61 ± 0.15 and 1.02 ± 0.28 for cD type and non-cD type clusters, respectively, at 90 per cent confidence level. Because the change in the Fe K *EW* should be less than a factor of 1.4 when the temperature decrease is ∼20 per cent, the Fe abundance must be significantly enhanced at the centre of cD type clusters. In contrast, such an abundance gradient is less significant among non-cD type clusters.

Table 2. Results of joint fitting of the GIS and SIS spectra at the centre region with the single-temperature variable abundance Raymond–Smith plasma model, including a free absorption (1T model).

Target	*kT* (keV)	Si (solar)	Fe (solar)	χ^2/ν
A2319	7.62 ± 0.64	1.31 ± 0.84	0.32 ± 0.07	1.16
Coma*	7.15 ± 0.53	1.05 ± 0.97	0.29 ± 0.07	1.03
A2256*	6.09 ± 0.35	1.30 ± 0.59	0.23 ± 0.05	1.20
A478	5.54 ± 0.18	1.00 ± 0.30	0.31 ± 0.03	1.30
Perseus	3.61 ± 0.04	0.69 ± 0.11	0.47 ± 0.02	2.27
A3571	5.82 ± 0.20	1.26 ± 0.53	0.40 ± 0.06	1.26
A85	4.57 ± 0.13	0.80 ± 0.42	0.50 ± 0.06	1.22
A1795	4.75 ± 0.11	0.79 ± 0.27	0.37 ± 0.03	1.32
A119*	4.99 ± 0.87	–	0.33 ± 0.23	1.02
A3558	5.07 ± 0.30	1.10 ± 0.66	0.47 ± 0.09	1.26
A2147*	4.13 ± 0.29	$0.49^{+0.86}_{-0.49}$	0.30 ± 0.10	1.13
A496	3.13 ± 0.07	0.77 ± 0.17	0.54 ± 0.04	1.51
A2199	3.70 ± 0.07	0.69 ± 0.24	0.48 ± 0.04	1.25
A4059	3.67 ± 0.10	0.70 ± 0.37	0.60 ± 0.07	1.16
AWM7	3.28 ± 0.11	0.97 ± 0.34	0.67 ± 0.09	1.25
A2634*	2.95 ± 0.32	2.33 ± 1.39	0.35 ± 0.21	1.03
MKW3s	3.30 ± 0.08	0.90 ± 0.23	0.45 ± 0.05	1.10
A2063	3.23 ± 0.12	0.73 ± 0.33	0.44 ± 0.07	1.11
Centaurus	2.20 ± 0.04	1.03 ± 0.15	1.10 ± 0.09	3.15
Hydra-A	3.26 ± 0.07	0.75 ± 0.21	0.40 ± 0.04	1.27
A1367*	3.15 ± 0.28	$0.15^{+0.33}_{-0.15}$	0.29 ± 0.08	1.14
A539*	2.86 ± 0.20	0.60 ± 0.37	0.33 ± 0.09	0.97
A1060*	3.25 ± 0.11	0.52 ± 0.32	0.32 ± 0.06	1.00
2A0335+096	2.43 ± 0.05	0.58 ± 0.15	0.44 ± 0.05	1.34
Virgo	1.62 ± 0.02	0.74 ± 0.08	0.61 ± 0.04	5.25
AWM4	2.28 ± 0.12	0.59 ± 0.43	0.53 ± 0.13	1.23
A400*	2.15 ± 0.25	0.49 ± 0.38	0.40 ± 0.21	1.17
A262	1.75 ± 0.06	0.72 ± 0.22	0.58 ± 0.10	1.25
MKW4s	1.70 ± 0.11	0.71 ± 0.34	0.46 ± 0.14	1.24
MKW4	1.57 ± 0.05	0.85 ± 0.20	0.75 ± 0.11	1.45
NGC 507	1.09 ± 0.02	0.52 ± 0.22	0.42 ± 0.12	1.32
Fornax	1.07 ± 0.02	0.40 ± 0.11	0.39 ± 0.07	1.24
NGC 5044	0.86 ± 0.01	0.19 ± 0.08	0.31 ± 0.03	1.72
HCG62	0.87 ± 0.02	0.16 ± 0.14	0.23 ± 0.05	1.37

* Non-cD type clusters.

3.2 Spectral fittings with a two-temperature plasma model

Metal abundances obtained by the 1T model fittings cannot be straightforwardly accepted, because the temperature decrease at the cluster centre indicates the existence of multiple temperature components there. We thus try to fit the central spectra with a two-temperature R–S model (2T R–S model) and constrain the metal abundance at the central region more reliably. Such 2T modelling is known to provide a reasonable approximation to the cluster spectra, even if they are made up of multiple temperature components (Fabian et al. 1994b). Furthermore, jointly using the *ROSAT*, *ASCA* GIS and *ASCA* SIS, Ikebe et al. (1999) studied the central region of the Centaurus cluster, where the cool emission component is most prominently visible. They have confirmed that the two-temperature (1.4 and 3.9 keV) modelling, first employed by Fukazawa et al. (1994), gives a fully consistent description of spatial and spectroscopic data from the three instruments. The two components are likely to be real, at least in this particular cluster. In addition, they have confirmed that the hot and cool components in the central region are both metal-enriched up to about 1 solar, and the abundances of the two components are consistent with being identical. We therefore adopt the 2T model not only as an empirical description of the *ASCA* spectra, but also as a physically meaningful representation of the ICM near the central regions of clusters.

In the 2T fitting, we fixed the temperature of the hot component to the spatially averaged cluster temperature obtained by Fukazawa

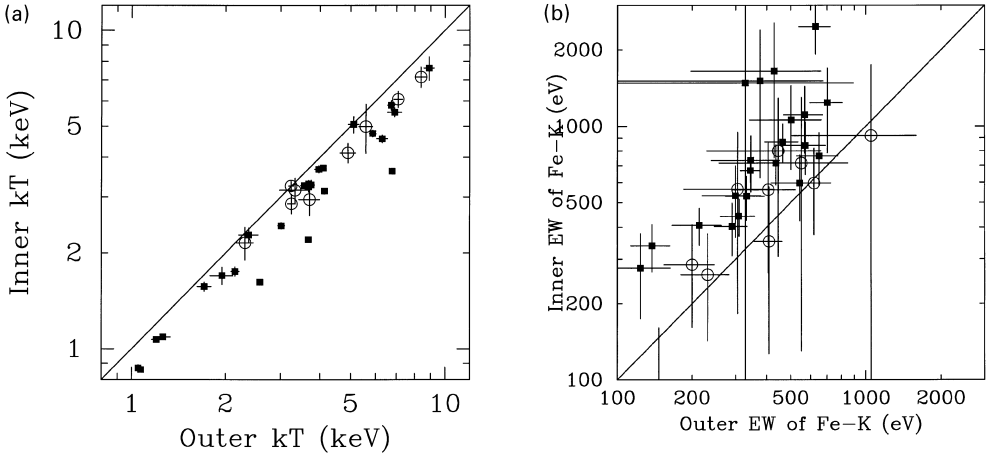

Figure 2. Plots of the fitting results between the central spectra and the outer region spectra. The left panel shows the temperature of the single temperature R–S model, and the right panel exhibits the equivalent widths of Fe K line. Filled squares and open circles represent cD type and non-cD type clusters, respectively. The straight line indicates equality between the two axes.

Table 3. The results obtained by jointly fitting the GIS and SIS spectra in the centre region with a two-temperature Raymond–Smith plasma model (2T model).

Target	$kT_{\rm cool}$ (keV)	Si (solar)	Fe (solar)	$N_{\rm cool}/N_{\rm hot}$†	χ^2/dof (bin number)
A2319	1.90 Fixed (9.2)	1.20 ± 0.68	0.32 ± 0.08	0.11 ± 0.05	1.17 (231)
Coma*	1.46 ± 0.58 (8.5)	0.84 ± 0.53	0.27 ± 0.08	0.11 ± 0.06	1.02 (219)
A2256*	2.00 ± 1.56 (7.0)	1.02 ± 0.48	0.23 ± 0.06	0.16 ± 0.12	1.19 (230)
A478	3.50 ± 0.88 (7.4)	0.88 ± 0.31	0.33 ± 0.04	0.67 ± 0.24	1.27 (214)
Perseus	2.25 ± 0.11 (6.5)	0.54 ± 0.09	0.40 ± 0.02	1.29 ± 0.11	1.79 (215)
A3571	1.83 ± 0.79 (7.0)	0.93 ± 0.40	0.39 ± 0.07	0.16 ± 0.06	1.20 (231)
A85	1.92 ± 0.65 (6.2)	0.73 ± 0.32	0.47 ± 0.07	0.35 ± 0.11	1.12 (231)
A1795	2.04 ± 0.63 (5.7)	0.73 ± 0.23	0.34 ± 0.04	0.22 ± 0.07	1.27 (231)
A119*	1.00 Fixed (5.6)	–	0.28 ± 0.22	<0.15	1.02 (76)
A3558	1.00 Fixed (5.2)	1.16 ± 0.66	0.46 ± 0.09	$0.01^{+0.04}_{-0.01}$	1.26 (231)
A2147*	1.00 Fixed (5.1)	1.16 ± 0.79	0.22 ± 0.10	$0.09^{+0.11}_{-0.09}$	1.18 (231)
A496	1.80 ± 0.14 (4.2)	0.67 ± 0.15	0.44 ± 0.05	0.62 ± 0.08	1.39 (217)
A2199	1.78 ± 0.32 (4.2)	0.66 ± 0.21	0.44 ± 0.05	0.17 ± 0.05	1.22 (231)
A4059	1.38 ± 0.25 (4.0)	0.73 ± 0.34	0.55 ± 0.07	0.08 ± 0.06	1.15 (231)
AWM7	1.83 ± 0.46 (3.8)	0.91 ± 0.32	0.61 ± 0.10	0.27 ± 0.13	1.25 (231)
A2634*	1.45 ± 0.66 (3.9)	1.55 ± 1.28	0.30 ± 0.19	$0.55^{+0.64}_{-0.55}$	1.03 (134)
MKW3s	1.45 ± 0.61 (3.5)	0.85 ± 0.22	0.42 ± 0.05	0.09 ± 0.07	1.09 (231)
A2063	1.64 ± 0.64 (3.6)	0.69 ± 0.31	0.41 ± 0.08	0.19 ± 0.12	1.12 (231)
Centaurus	1.37 ± 0.02 (3.8)	0.95 ± 0.12	0.79 ± 0.06	1.02 ± 0.09	1.76 (218)
Hydra-A	2.15 ± 0.90 (3.6)	0.71 ± 0.21	0.38 ± 0.05	0.28 ± 0.24	1.30 (231)
A1367*	2.04 ± 0.83 (3.3)	<0.73	0.29 ± 0.08	0.16 ± 0.13	1.10 (231)
A539*	1.00 Fixed (3.2)	0.74 ± 0.43	0.32 ± 0.10	$0.08^{+0.11}_{-0.08}$	0.98 (227)
A1060*	1.00 Fixed (3.2)	0.49 ± 0.31	0.31 ± 0.06	<0.04	1.00 (231)
2A0335+096	1.42 ± 0.07 (3.1)	0.47 ± 0.13	0.34 ± 0.04	0.65 ± 0.09	1.22 (220)
Virgo	1.25 ± 0.02 (2.7)	0.78 ± 0.08	0.58 ± 0.03	1.44 ± 0.12	2.27 (198)
AWM4	1.14 ± 0.23 (2.3)	0.56 ± 0.42	0.48 ± 0.15	$0.11^{+0.21}_{-0.11}$	1.20 (180)
A400*	1.00 Fixed (2.5)	0.81 ± 0.46	0.27 ± 0.16	$0.01^{+0.12}_{-0.01}$	1.19 (137)
A262	1.11 ± 0.07 (2.1)	0.82 ± 0.23	0.61 ± 0.11	0.25 ± 0.16	1.11 (187)
MKW4s	0.88 ± 0.05 (2.0)	0.90 ± 0.32	0.61 ± 0.16	0.16 ± 0.08	0.96 (141)
MKW4	1.15 ± 0.19 (1.8)	0.91 ± 0.21	0.80 ± 0.13	0.33 ± 0.28	1.48 (164)
NGC 507	1.09 ± 0.09 (1.3)	0.61 ± 0.26	0.48 ± 0.20	$4.51^{+23.81}_{-4.51}$	1.24 (119)
Fornax	0.87 ± 1.05 (1.2)	0.40 ± 0.16	0.44 ± 0.10	0.48 ± 0.24	1.25 (142)
NGC 5044	0.84 ± 0.01 (1.1)	0.20 ± 0.05	0.33 ± 0.05	4.83 ± 4.42	1.79 (137)
HCG62	0.83 ± 0.10 (1.0)	0.25 ± 0.11	0.30 ± 0.07	$0.47^{+0.56}_{-0.47}$	1.29 (117)

* Non-cD type clusters.
† The ratio of the emission measure of the cool component to that of the hot component.

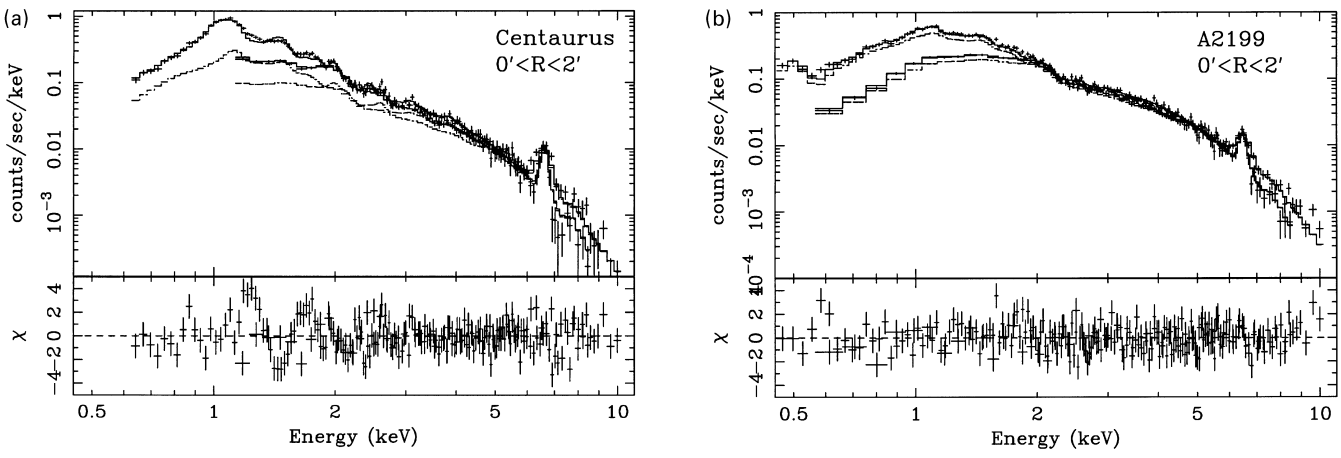

Figure 3. The spectra at the central regions and their joint fits with the 2T R–S model assuming variable abundance ratios. Left and right panels represent the Centaurus cluster and A2199, respectively. The solid line represents the total best-fitting model, and the dashed line represents the hot component.

et al. (1998). Metal abundances were assumed to be the same between the two components, because the data quality is usually not adequate to determine the abundances and normalization of the cool component independently. The ratio of normalization of the cool component to the hot component was constrained to be the same between the GIS and SIS. Thus the free parameters are normalizations of the two components, the cool-component temperature, and the abundances and hydrogen column density, which are common to both components. We left the abundance ratios partially free to deviate from the solar values, as described in the previous subsection. The temperature of the cool component is poorly constrained for some clusters, and in such a case we

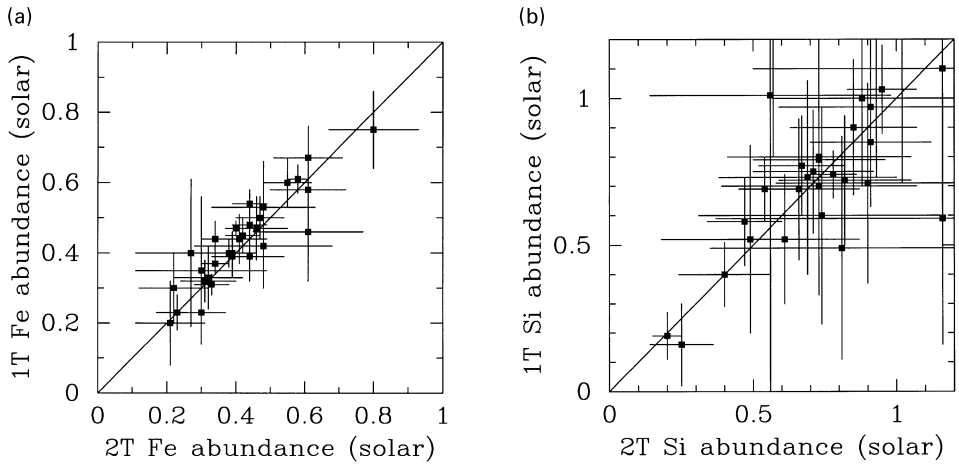

Figure 4. The comparison of Fe (left panel) and Si (right panel) abundances between 2T and 1T model fits. The straight line indicates equality between the two quantities.

Table 4. Results of joint fitting of the GIS and SIS spectra with the two-temperature variable abundance plasma model plus two additional Gaussians. The values in the parentheses are the best-fitting values without additional Gaussians.

Target	Model	Line energy (keV)	Line EW (eV)	Si (solar)	Fe (solar)	χ^2/dof (bin number)
Perseus	R–S	1.29 ± 0.03, 1.70 ± 0.03	7.6, 12	0.66 ± 0.10	0.43 ± 0.03	1.57
				(0.54 ± 0.09)	(0.40 ± 0.02)	(1.79)
	Mekal	1.24 ± 0.03, 1.71 ± 0.03	9.2, 8.9	0.72 ± 0.11	0.45 ± 0.03	1.60
				(0.58 ± 0.11)	(0.43 ± 0.02)	(1.78)
	Masai	1.30 ± 0.03, 1.71 ± 0.03	11, 13	0.75 ± 0.11	0.45 ± 0.03	1.68
				(0.57 ± 0.08)	(0.39 ± 0.02)	(1.99)
Centaurus	R–S	1.24 ± 0.02, 1.71 ± 0.03	29, 33	1.22 ± 0.16	0.90 ± 0.07	1.40
				(0.95 ± 0.12)	(0.79 ± 0.06)	(1.76)
	Mekal	1.22 ± 0.03, 1.75 ± 0.03	36, 22	1.26 ± 0.22	0.83 ± 0.09	1.41
				(0.90 ± 0.14)	(0.73 ± 0.05)	(1.71)
	Masai	1.25 ± 0.03, 1.71 ± 0.03	39, 33	1.04 ± 0.16	0.86 ± 0.08	1.49
				(0.68 ± 0.09)	(0.68 ± 0.05)	(1.90)
Virgo	R–S	1.26 ± 0.02, 1.67 ± 0.02	34, 23	0.97 ± 0.10	0.66 ± 0.04	1.69
				(0.78 ± 0.08)	(0.58 ± 0.03)	(2.27)
	Mekal	1.21 ± 0.03, 1.75 ± 0.03	26, 22	1.02 ± 0.09	0.55 ± 0.03	1.48
				(0.82 ± 0.09)	(0.49 ± 0.03)	(2.04)
	Masai	1.26 ± 0.03, 1.71 ± 0.03	28, 24	0.90 ± 0.11	0.71 ± 0.05	1.86
				(0.61 ± 0.05)	(0.56 ± 0.03)	(2.31)

fixed the temperature to an appropriate value, as shown in Table 3. The other parameters are not affected significantly by doing that.

The best-fitting parameters of these 2T fits are shown in Table 3, and the fit examples are shown in Fig. 3. We can see that the cool component explains the strong Fe L line complex, and the Fe K line is mainly contributed from the hot component. The 2T model gives significantly smaller values of reduced χ^2 than the 1T model in half the clusters, and the improvement of fitting is confirmed to be significant by an F test at the 90 per cent confidence level. The drop in χ^2 is particularly noticeable in clusters with central spectra that were not described well with the 1T R–S model. Therefore, the central spectra of half the clusters need at least two temperature components. Nevertheless, the best-fitting abundances of Fe and Si are not very different between the 1T and 2T fits, as shown in Fig. 4. This is because the Fe K and Si K lines are mostly contributed by the hot component. We also confirmed that the cooling-flow model gives almost the same results as the 2T model (Fukazawa 1997), in agreement with Fabian et al. (1994b).

There are four clusters (Virgo, Centaurus, Perseus and the NGC 5044 group) exhibiting reduced χ^2 values of larger than 1.5 even in the 2T fit. For the former three clusters, common residual features are seen around 1.3 and 1.7 keV (Fig. 3). The residuals do not disappear even when we utilize other plasma codes such as the Mewe–Kaastra–Liedahl code (Mekal code: Mewe, Gronenschild & van der Oord 1985; Liedahl, Osterheld & Goldstein 1995) and the Masai code (Masai 1984), or the available homogeneous cooling-flow model (Mushotzky & Szymkowiak 1988). These are probably caused by uncertainties of the Fe L line modelling for the cool component; the models are overpredicting emission lines at ~1.4 keV. When introducing two artificial Gaussians to account for these residuals, the fits improve as shown in Table 4. The centre energies of the two Gaussians are nearly coincident at ~1.25 and ~1.70 keV for the three clusters, while the equivalent widths are different among them. The abundances change by ~20 per cent when the two Gaussians are included, but the central abundance increase remains significant.

For the NGC 5044 group, the residual is mainly seen around Fe

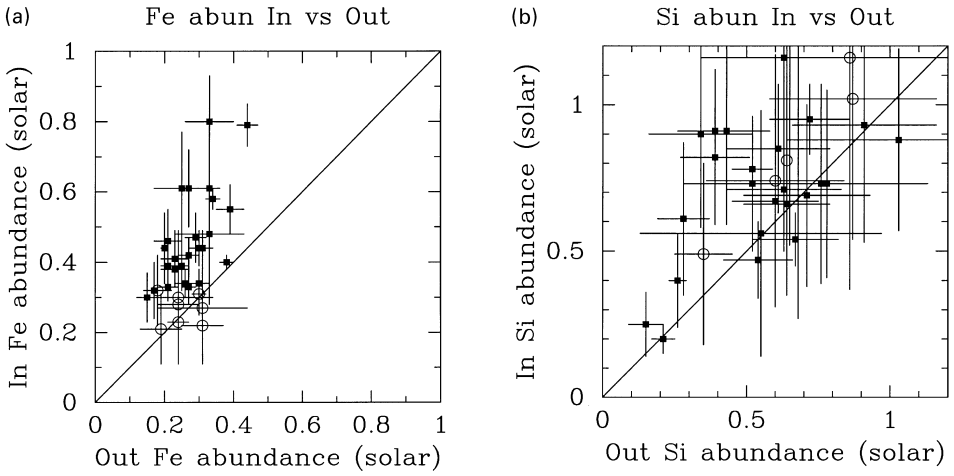

Figure 5. The comparison of Fe (left panel) and Si (right panel) abundances between the centre and the outer regions. The results are obtained by simultaneous fitting of the GIS and SIS spectra with the 2T R–S model. Meaning of symbols is the same as in Fig. 2. The straight line indicates equality between X and Y axes.

L lines, and hence the large χ^2 is caused by the uncertainty in the Fe L line modelling around $kT = 1$ keV. The uncertainty of Fe abundances for clusters with $kT = 1$ keV is described in the next subsection.

As seen in Table 3, several clusters show quite high central Fe abundances up to 0.6–0.8 solar, such as Centaurus, Virgo, AWM7, A262, MKW4s and MKW4. This reconfirms the central abundance increases that have already been reported for Centaurus (Fukazawa et al. 1994), Virgo (Matsumoto et al. 1996) and AWM7 (Xu et al. 1997). We compare the central abundances of Fe and Si with the spatially averaged ones in Fig. 5. The central Fe abundances of cD type clusters are systematically higher by a factor of 1–3 than their spatially averaged values, while those of non-cD type clusters are almost the same as their spatially averaged ones. The Si abundance is significantly higher at the centre in several cD type clusters, although definite statements cannot be made on many other clusters.

In summary, we have found that the metal abundances at the central regions are higher than those in the outer region in most cD type clusters, independently of the temperature structure. Therefore, it can be said that the central abundance increment is a common phenomenon among cD type clusters. In contrast, non-cD type clusters do not exhibit such an abundance gradient. Hereafter, we quote the metal abundances obtained by the 2T R–S model for clusters requiring the cool component, and those obtained by the 1T model for other clusters.

3.3 Properties of the central metal abundances

As non-cD type clusters do not a exhibit significant abundance gradient as described in Section 3.1, hereafter we limit our attention to cD type clusters only. We plot the central Fe and Si abundances of cD type clusters in Fig. 6, and their ensemble-averaged abundances in Fig. 7, against the spatially averaged temperature obtained by Fukazawa et al. (1998). We also plot results given by the Mekal and Masai codes, in order to investigate the dependence on the plasma codes (e.g. Fabian et al. 1994b; Fukazawa et al. 1996) in Fig. 7. To compare the central metallicity with that of the outer region, in Fig. 7 we further plot the sample-averaged abundance of the outer region determined by Fukazawa et al. (1998) using the R–S code.

As shown in Fig. 6, most cD type clusters, even hot ones, have higher Fe abundances than the spatially averaged values of 0.3 solar (Fukazawa et al. 1998). The ensemble-averaged Fe abundances of cD type clusters (Fig. 7 left) exhibit a clear negative correlation with the averaged ICM temperature, regardless of the plasma codes. While this behaviour is distinct from that of the outer region Fe abundance (Fukazawa et al. 1998), it is quite similar to the trend of the emission-weighted value obtained by *Ginga* (Hatsukade 1989; Tsuru 1992). Therefore, we infer that the *Ginga* results were affected by the central metal-enriched region. Actually, in Fig. 8 we derived emission-weighted Fe abundances by integrating the GIS data within 15 arcmin of the cluster centre, which reproduce the *Ginga* results.

Below $kT = 1.5$ keV, the ensemble-averaged Fe abundances differ considerably among plasma codes because of large uncertainties in the Fe L modelling, although the central increase in the Fe abundance is robust.

The ensemble-averaged Si abundance at the centre also exhibits a noticeable difference from the outer region values shown in Fukazawa et al. (1998); instead of showing the positive correlation with the ICM temperature seen in the outer region, the central Si abundance stays rather constant and high, 0.6–1.0 solar, except in the coolest objects. This is because cooler cD clusters exhibit stronger Si abundance increases (by 0.2–0.3 solar) at the centre, as clearly seen in Fig. 7.

To compare the spatial behaviour of Fe and Si more directly, we plot the central region abundances obtained here and the outer region abundances derived in Fukazawa et al. (1998), separately for cooler ($kT < 3$ keV) and hotter ($3.5 < kT < 5$ keV) clusters in Fig. 9; these two groupings are represented by the Virgo cluster (Matsumoto et al. 1996) and the Centaurus cluster (Fukazawa et al. 1994; Ikebe 1995), respectively. Thus, abundances of Si and Fe are seen to correlate positively in general. In cooler clusters, the Si and Fe abundances increase towards the centre quite similarly, both by 0.2–0.4 solar, roughly keeping the Si/Fe ratio of 1–1.5. This trend agrees with the results on the Virgo cluster (Matsumoto et al. 1996). On the other hand, in hotter clusters, Fe exhibits larger abundance increments towards the centre than Si; Fe increases typically by 0.1–0.4 solar and Si by <0.2 solar. The Centaurus cluster gives the best example of such behaviour, as specified in Fig. 9. In

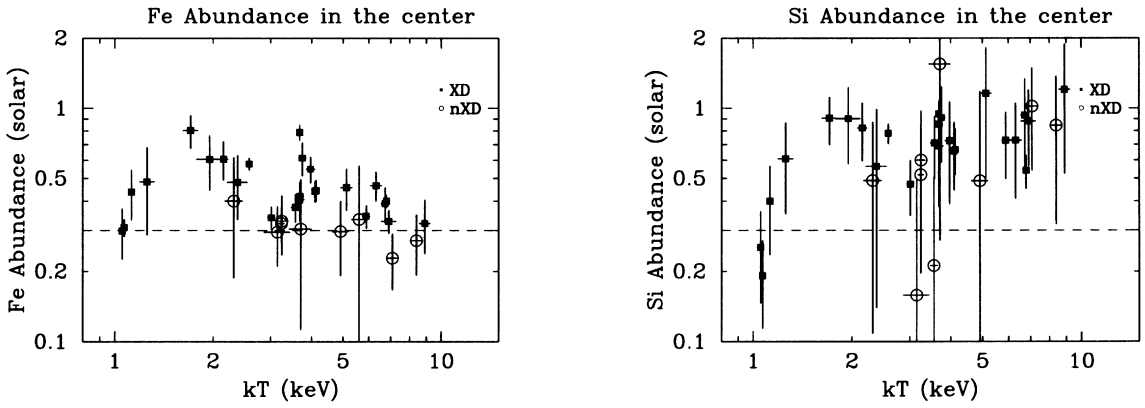

Figure 6. The Fe (left) and Si (right) abundances in the central regions, plotted as a function of the spatially averaged ICM temperature obtained in Fukazawa et al. (1998). The GIS and the SIS data have been utilized jointly. Filled squares represent cD type clusters, while open circles show non-cD type clusters. The horizontal dashed line represents 0.3 solar abundance level. The metal abundances shown in this figure are all based on the R–S model.

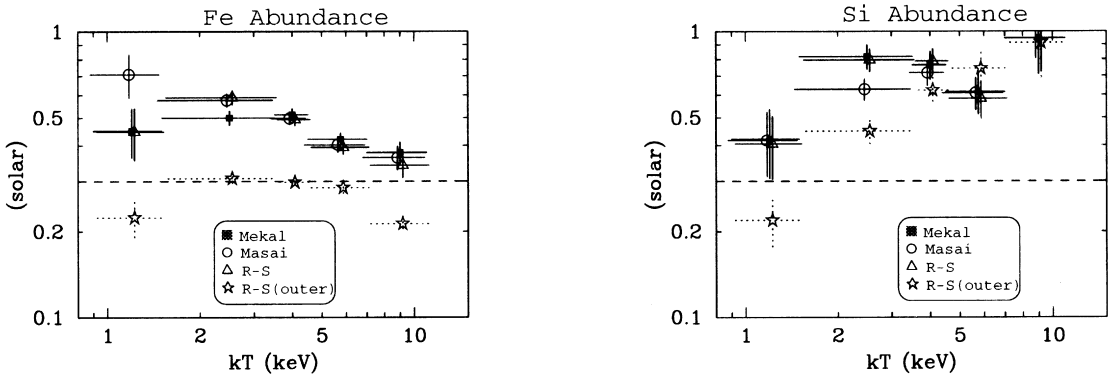

Figure 7. The ensemble-averaged Fe and Si abundances in the centre regions of cD type clusters, plotted as a function of the spatially averaged ICM temperature. Different symbols specify the three plasma codes. For comparison, the outer region abundances (Fukazawa et al. 1998) obtained by the R–S code are also plotted with star symbols. The horizontal dashed line represents the 0.3 solar abundance level.

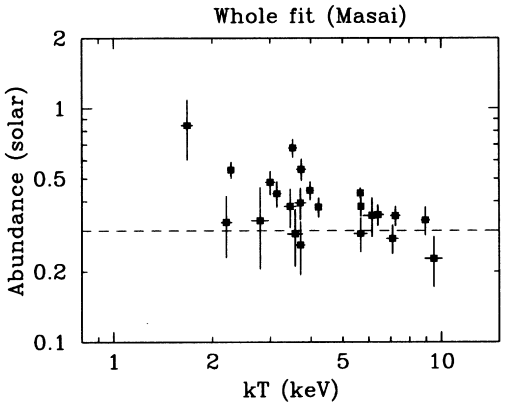

Figure 8. The Fe abundances obtained by fitting the GIS spectra integrated over the whole cluster region. The single-temperature Masai model is utilized, since *Ginga* results were usually obtained by using this model. Only clusters observed by *Ginga* are plotted against the ICM temperature.

other words, the regions near cD galaxies exhibit roughly solar-like Si/Fe ratios regardless of the cluster richness, whereas the outer cluster regions exhibit progressively higher Si/Fe ratios towards richer clusters.

4 DISCUSSION

4.1 The origin of excess metal abundances around cD galaxies

Prior to the present paper, several examples of Fe abundance increase around cD galaxies had been reported based on the *Ginga* and early *ASCA* observations (e.g. Koyama et al. 1991; Fukazawa et al. 1994; Ohashi et al. 1995; Matsumoto et al. 1996; Xu et al. 1997; Kikuchi et al. 1999). We have shown that this phenomenon is quite common among cD type clusters: most of them exhibit statistically significant Fe abundance increases around their cD galaxies. As shown in Fig. 7, the Fe abundance increment is larger (by 0.2–0.4 solar) in cooler clusters than in hotter ones (by 0.1–0.2 solar). This phenomenon occurs typically within $100\,h_{50}^{-1}$ kpc from the cD galaxy; in the Centaurus (Ikebe 1995) and Virgo (Matsumoto et al. 1996) clusters, the spatial scale of this phenomenon has been measured to be 30–$60\,h_{50}^{-1}$ kpc, which is comparable to the size of the cD galaxy. Another intriguing fact is that the metallicity of non-cD type clusters stays nearly constant even at the cluster centre.

In the intracluster space, heavy ions could condense towards the bottom of gravitational potential, producing metallicity gradients. However, this process is expected to take place on time-scales much longer than the age of the Universe (Sarazin 1988). We therefore regard the observed metal increment as caused by

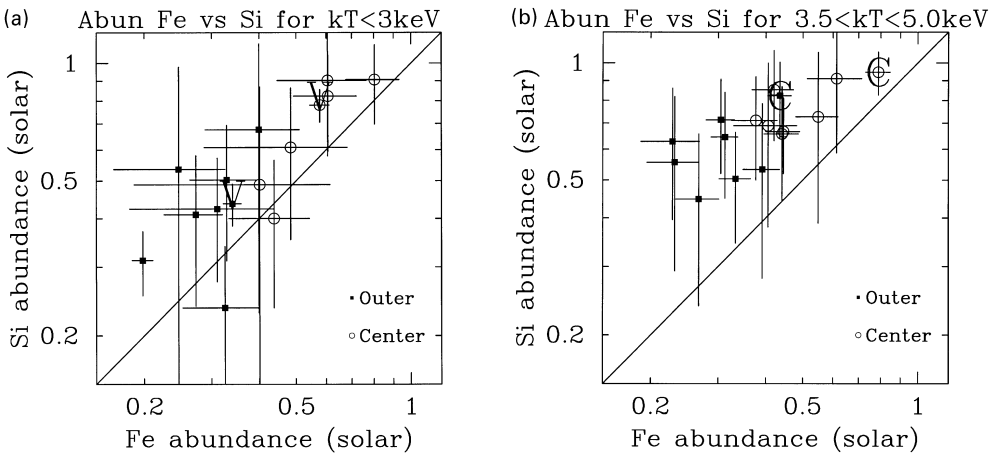

Figure 9. The Si abundances against the Fe abundances in cD type clusters, plotted separately for lower (left panel) and higher (right panel) temperature clusters. Open circles and filled squares represent the abundances in the central and outer regions, respectively. The 'V' and 'C' symbols represent the Virgo and Centaurus clusters, respectively.

somehow enhanced ejection of heavy elements from member galaxies near the cluster centre, and/or by a better metal confinement, rather than by any microscopic process.

One possible mechanism of enhanced metal ejection is ram-pressure stripping of metal-rich interstellar gas of member galaxies. However, this idea fails to explain the difference seen between clusters of cD types and non-cD types, and fails to explain how the metallicity enhancement is limited to the vicinity of the cD galaxy. Therefore, we infer that the excess metallicity around cD galaxies is caused by metal-rich gas ejected from cD galaxies themselves.

We have discovered that the central excess metals around cD galaxies exhibit roughly solar-like chemical composition, compared with the Si-rich abundance in the outer region of rich clusters. In other words, the central regions of cD type clusters are probably more heavily contributed to by SNe Ia than their outer regions. Although the central abundances could be subject to resonance line scattering, we do not find any such evidence. As SNe II should be rare in elliptical galaxies (e.g. van den Bergh & Tammann 1991), the SNe Ia like chemical composition provides strong support to our view that the excess metals in the centre of cD type clusters came from cD elliptical galaxies.

In that case, can the amount of excess metals at the centre be provided by the cD galaxy alone? As shown by Renzini et al. (1993), a giant elliptical galaxy can supply to the ICM, over its lifetime, a large amount of iron, the mass of which is comparable to the total iron mass now contained in its stellar interior. Although it is rather difficult in general to resolve the central abundance profile accurately enough to constrain the excess iron mass, Ikebe et al. (1999) has successfully determined the central Fe abundance radial profile in the Centaurus cluster as $A\exp(-r/R_Z)+B$, where $A=1.0$ solar, $B=0.15$ solar, and $R_Z=80\,h_{50}^{-1}$ kpc. Utilizing this empirical form and the ICM density distribution of each cluster obtained in Fukazawa (1997), we calculate the iron mass within $150\,h_{50}^{-1}$ of the centre for our sample clusters. We adjusted A so as to reproduce the observed central abundance, while we set $B=0.15$ and $R_Z=80\,h_{50}^{-1}$ kpc after the Centaurus cluster. As shown in Fig. 10, the iron mass at the cluster centre is at most $7\times10^9\,M_\odot$ for any cluster. Such a mass can be supplied by the cD galaxy (Renzini et al. 1993).

In conclusion, we are just observing the accumulation of metal ejection from the cD galaxy into the ICM. This supports the general view of chemical evolution of clusters of galaxies; metals in the ICM are processed in the stellar interior in member galaxies and ejected into interstellar/intergalactic space. One consequence of this result is that, when we study cosmological evolution of the ICM metallicity by observing distant clusters, we must carefully resolve their central regions, where the metallicity may be enhanced.

4.2 Differences between cD type and non-cD type clusters

We found a significant difference in the central ICM metallicity between cD type and non-cD type clusters; the former exhibit a significant metal increment, while the latter do not. This generalizes the suggestion by Tamura et al. (1996) that clusters with one central dominant galaxy tend to exhibit an abundance increase at the centre, and clusters with several galaxies of similar dominance do not. In addition, because cD type clusters are usually classified as cooling-flow clusters, our results confirm the claim by Allen & Fabian (1998) that cooling-flow clusters tend to show abundance increases at the centre. However, many non-cD type clusters also have a few (typically two) giant elliptical galaxies in the cluster centre, and their total stellar content is almost the same as that of a single cD galaxy. Therefore, the difference between the two types of cluster cannot be attributed to the difference in the stellar mass density. What, then, produces this difference?

Considering the properties of galaxies at the centre of cD type and non-cD type clusters, we can make a phenomenological statement that the metal abundance increase is seen around a central giant elliptical galaxy when it is not neighboured by other giant ellipticals within 50–$150\,h_{50}^{-1}$ kpc. This was first pointed out by Tamura et al. (1996) through comparison of a non-cD type cluster, A1060, with several cD type clusters.

A likely explanation of the above effect is that the central giant galaxies in a non-cD type cluster are under strong tidal interactions with each other, so that their metal-rich ejecta are highly disturbed and become turbulent (Tamura et al. 1996). Furthermore, such galaxies must be moving with respect to the ICM with a velocity comparable to the sound velocity in the ICM (Ikebe et al. 1997), so that their interstellar media are subject to ram-pressure stripping by the surrounding ICM. Through these processes, the excess iron may be easily mixed into the

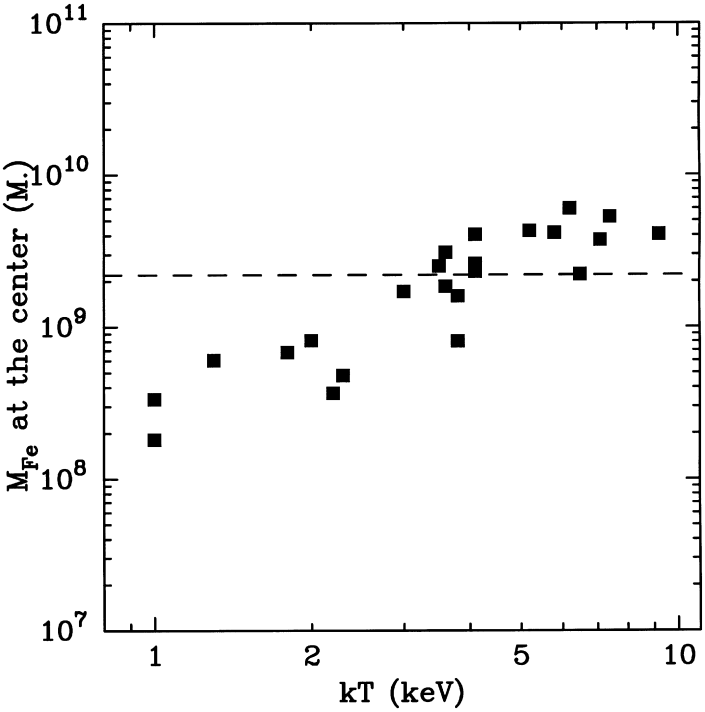

Figure 10. The Fe mass within $150\,h_{50}^{-1}$ of the cluster centre, assuming the Fe abundance radial profile obtained for the Centaurus cluster, $A_0 \exp(-r/R_Z) + 0.15$ solar, where A_0 is adjusted so that the emission-measure weighted central abundance becomes the observed value and $R_Z = 80\,h_{50}^{-1}$ kpc.

surrounding metal-poor ICM and may become diluted. In other words, the metals produced in these galaxies may be quickly transported into the intracluster space, as is probably the case with ordinary ellipticals in clusters (Matsushita 1997). A cD galaxy is considered to sit at the bottom of the cluster potential, approximately at rest with respect to the surrounding ICM. In such a case, the ram-pressure stripping would not work. In addition, a high ambient pressure caused by the surrounding ICM will suppress the escape of metal-rich supernova products from the cD galaxy.

4.3 The relation between the cluster temperature and Fe abundance

Our results for the centre of cD type clusters reveal a negative correlation of the Fe abundance with the cluster temperature (Fig. 7). To understand this property, let us consider the Fe mass rather than the Fe abundance at the cluster centre (see Fig. 10). Interestingly, the Fe mass around the cluster centre exhibits the opposite tendency, lower Fe mass for lower temperature clusters, although the Fe mass seems to be constant above $kT > 4\,\mathrm{keV}$. This different behaviour of the iron mass is caused by the lower ICM mass within $150\,h_{50}^{-1}$ kpc of the centre in lower temperature clusters. That is, the amount of excess iron around cD galaxies in fact decreases as the cluster becomes poorer, but the total amount of ICM in the central region deceases more steeply toward poorer systems. As a consequence, poorer cD clusters tend to exhibit a higher Fe abundance in their central regions.

In Fig. 10, we see a steep decrease of the Fe mass toward lower temperature clusters. As the total amount of Fe produced by a cD galaxy should be independent of the cluster richness, Fig. 10 implies that most of the metals ejected from a cD galaxy have already spread over into the wide intracluster space, and this effect is stronger in poorer clusters, presumably because of the shallower potential. This might smoothly connect to the even stronger 'metal-escape' effect found by Matsushita (1997) for non-cD elliptical galaxies.

ACKNOWLEDGMENTS

The authors are grateful to the *ASCA* team for their help in the spacecraft operation and calibration. This research was supported in part by the Grants-in-Aid for the Center-of-Excellence (COE) Research of the Ministry of Education, Science, and Culture in Japan (07CE2002).

REFERENCES

Albert C. E., White R. A., Morgan W. W., 1977, ApJ, 211, 309
Allen S. W., Fabian A. C., 1998, MNRAS, 297, L63
Anders E., Grevesse N., 1989, Geochim. Cosmochim. Acta., 53, 197
Arimoto N., Yoshii Y., 1987, A&A, 173, 23
Arnaud M., Rothenflug R., Boulade O., Vigroux L., Vangioni-Flam E., 1992, A&A, 254, 49
Awaki H., Koyama K., Kunieda H., Takano S., Tawara Y., Ohashi T., 1991, ApJ, 366, 88
Awaki H. et al., 1994, PASJ, 46, L65
Bahcall N. A., 1977, ApJ, 217, L77
Edge A. C., Stewart G. C., Fabian A. C., 1992, MNRAS, 258, 177
Ezawa H., Fukazawa Y., Makishima K., Ohashi T., Takahara F., Xu H., Yamasaki N. Y., 1997, ApJ, 490, L33
Fabian A. C., Nulsen P. E. J., Canizares C. R., 1984, Nat, 310, 733
Fabian A. C., Crawford C. S., Edge A. C., Mushotzky R. F., 1994a, MNRAS, 267, 779
Fabian A. C., Arnaud K. A., Bautz M. W., Tawara Y., 1994b, ApJ, 436, L63

Finoguenov A., Ponman T. J., 1999, MNRAS, 305, 325
Fukazawa Y., 1997, PhD thesis, Univ. Tokyo
Fukazawa Y., Ohashi T., Fabian A. C., Canizares C. R., Ikebe Y., Makishima K., Mushotzky R. F., Yamashita K., 1994, PASJ, 46, L55
Fukazawa Y. et al., 1996, PASJ, 48, 395
Fukazawa Y., Makishima K., Tamura T., Ezawa H., Xu H., Ikebe Y., Kikuchi K., Ohashi T., 1998, PASJ, 50, 187
Hatsukade I., 1989, PhD thesis, Osaka Univ.
Ikebe Y., 1995, PhD thesis, Univ. Tokyo
Ikebe Y. , Fukazawa Y., Tamura T., Makishima K., Ohashi T., 1997, in Makino F., Mitsuda K., eds, X-Ray Imaging and Spectroscopy of Cosmic Hot Plasmas. Universal Academy Press, Tokyo, p. 57
Ikebe Y., Makishima K., Fukazawa Y., Tamura T., Xu H., Ohashi T., 1999, ApJ, 525, 58
Jones C., Forman W., 1984, ApJ, 276, 38
Kikuchi K., Furusho T., Ezawa H., Yamasaki N., Ohashi T., Fukazawa Y., Ikebe Y., 1999, PASJ, 51, 301
Koyama K., Takano S., Tawara Y., 1991, Nat, 350, 135
Liedahl D., Osterheld A., Goldstein W., 1995, ApJ, 438, L115
Loewenstein M., Mushotzky R. F., Tamura T., Ikebe Y., Makishima K., Matsushita K., Awaki H., Serlemitsos P. J., 1994, ApJ, 436, L75
Makishima K. et al., 1996, PASJ, 48, 171
Masai K., 1984, Ap&SS, 98, 367
Matsumoto H., Koyama K., Awaki H., Tomita H., Tsuru T., Mushotzky R. F., Hatsukade I., 1996, PASJ, 48, 201
Matsushita K., 1997, PhD thesis, Univ. Tokyo
Matsushita K., Makishima K., Rokutanda E., Yamasaki N. Y., Ohashi T., 1997, ApJ, 488, L125
Mewe R., Gronenschild E. H. B. M., van den Oord G. H. J., 1985, A&AS, 62, 197
Morgan W. W., Kayser S., White R. A., 1975, ApJ, 199, 545
Mushotzky R. F., Szymkowiak A. E., 1988, in Fabian A. C., eds, Cooling Flows in Clusters and Galaxies. Kluwer Academic Publishers, Cambridge, p. 53
Mushotzky R. F., Loewenstein M., Awaki H., Makishima K., Matsushita K., Matsumoto H., 1994, ApJ, 436, L79
Mushotzky R. F., Loewenstein M., Arnaud K. A., Tamura T., Fukazawa Y., Matsushita K., Kikuchi K., Hatsukade I., 1996, ApJ, 466, 686
Ohashi T., Fukazawa Y., Ikebe Y., Esawa H., Tamura T., Makishima K., 1995, in Makino F., Ohashi T., eds, New Horizon of X-ray Astronomy. Universal Academy Press, Tokyo, p. 273
Ohashi T. et al., 1996, PASJ, 48, 157
Raymond J. C., Smith B. W., 1977, ApJS, 35, 419
Renzini A., Ciotti L., D'Ercole A., Pellegrini S., 1993, ApJ, 419, 52
Rood H. J., Sastry G. N., 1971, PASP, 83, 313
Sarazin C. L., 1988, X-Ray Emission from Clusters of Galaxies. Cambridge Univ. Press, Cambridge
Scott T. S., Robertson J. W., Tarenghi M., 1977, A&A, 59, 23
Struble M. F., Rood H. J., 1987, ApJS, 63, 555
Takahashi T. et al., 1995, ***ASCA*** News, 3, 34
Tamura T. et al., 1996, PASJ, 48, 671
Tanaka Y., Inoue H., Holt S. S., 1994, PASJ, 46, L37
Tsuru T., 1992, PhD thesis, Univ. Tokyo
van den Bergh S., Tammann G. A., 1991, ARA&A, 29, 363
White D. A., Jones C., Forman W., 1998, MNRAS, 292, 419
Xu H., Ezawa H., Fukazawa Y., Kikuchi K., Makishima K., Ohashi T., Tamura T., 1997, PASJ, 49, 9
Yamashita K., 1992, in Tanaka Y., Koyama K., eds, Frontiers of X-ray Astronomy. Univ. Academy Press, Tokyo, p. 475

This paper has been typeset from a TEX/LATEX file prepared by the author.